Techno-economic optimization of a modular CSP tower plant of 5 MW$_{el}$

TESI MAGISTRALE IN ENERGY ENGINEERING

EXECUTIVE SUMMARY

Corradini, Luca, 10571936

Advisor:
Prof. Giampaolo Manzolini

Co-advisors:
Giancarlo Gentile
Ettore Morosini

Academic year:
2021-22

Abstract: This thesis work compares different modular concentrated solar power (CSP) tower plants with their corresponding single field counterparts. For the modular configurations different heliostat dispositions and module sizes are investigated. Two ranges of operating temperatures are also considered. Sodium is adopted as heat transfer fluid (HTF), advanced molten salts are used as storage media, and a supercritical CO_2 cycle is considered for the 5 MW$_{el}$ power block. Solar field, receiver, piping system, thermal energy storage (TES) system and power block are modelled to design and evaluate the performances of the plant. The piping system model is developed as part of this thesis work. For each configuration, tower height and receiver area are determined by optimization of the levelized cost of heat (LCOH). The solar multiple and the TES size of each configuration are determined by optimization of the levelized cost of electricity (LCOE). The identified best modular plant, consisting of 10 polar field modules, each one of 5 MW$_{th}$ of incident power on the receiver, achieves a LCOE value of 143.6 $/MWh, a reduction of 6.5 % with respect to the LCOE provided by the corresponding best single field plant.

1 Introduction

The present work focuses on the techno-economic optimization of a modular concentrated solar power (CSP) tower plant and its comparison with a single tower plant. The aim of the work is to evaluate the possible advantages and disadvantages of adopting a modular configuration with respect to a single solar field plant, in order to identify the best design options and to orient future research and decision making when designing CSP plants. The concept of modular solar tower plants is still in a very early stage of development: very few research articles are available in literature and very few pilot projects have been realized. A study by *Lim et al. (2017)* [1] underlines the possibilities of the modular approach for CSP plants. A study by *Crespo et al. (2020)* [2] points out the advantages of splitting the size of the heliostat field-receiver subsystems to avoid the impact on performance of enlarging surrounding fields, particularly in hazy locations. A study from *Tyner et al. (2013)* [3] proposes the design of a molten salt system based on a 50-MW$_{th}$ module comprised of a tower-mounted molten salt receiver. A study by *Crespo et al. (2018)* [4] considers a surrounded field reference plant of 100 MW with 8 hours of storage at 38º northern latitude. The performances of this reference plant are compared with 2x50 MW and 3x33 MW north field plants. Another study, by *Puppe et al. (2018)* [5], investigates a hypothetical 125 MW$_{el}$ molten salt tower plant. Five smaller solar fields instead of one big solar field, feeding the same storage system and power block are investigated. One of the few pilot plants involving modular CSP tower technology was the Lake Cargelligo solar thermal project. It consisted of a 3MW$_{el}$ steam turbine generator, and it was dismantled in 2016 after more than 25,000 hours of operation [6]. In 2009 eSolar begun the construction of a modular solar tower power facility including two modules and a turbine generator of 5 MW. The plant remained operational until 2014. The only operational modular solar tower pilot plant is Vast Solar Jemalong power facility in Australia. This plant comprises 5 modules using liquid sodium as heat transfer fluid and storage media for a 3h storage capacity and a 1.1 MW steam turbine [7].

2 Modelling

In order to investigate modular solar tower systems different tools are employed and developed to model the different subsystems of the plant (
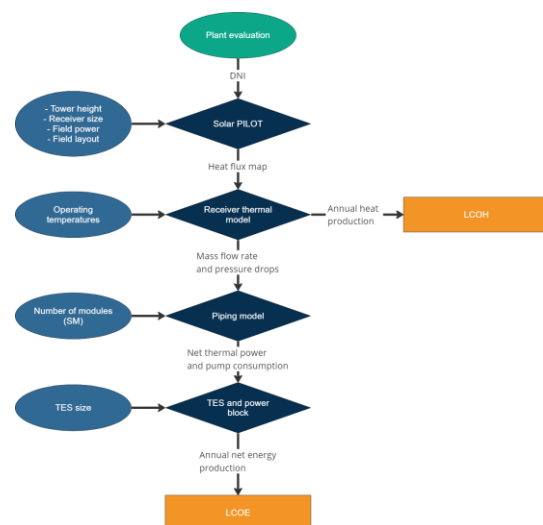
Figure 1).

Figure 1 Methodology flow chart

2.1. Solar field

For the study of the optical efficiency of the concentrating system the software SolarPILOT is employed [8]. SolarPILOT includes the ability to generate field layouts in a variety of patterns or land constraints, conduct detailed optical performance simulations and conduct parametric analyses. For any performance simulation SolarPILOT provides total

heliostat area, heliostat number, power incident on the field and power delivered to the receiver, heat flux map (HFM) of the receiver, optical efficiency.

2.2. Receiver

The HFM of the receiver provided by SolarPilot, is used as input for the receiver model coded in Matlab® [9]. Two different receiver models are employed: one billboard receiver model for the solar fields with polar layout, and one external cylindrical receiver model for the solar fields with surrounded layout. These models allow to simulate the steady state behaviour of the receiver accounting for receiver characteristics, HTF type, heat flux distribution, ambient conditions, and for reflective, radiative, and convective thermal losses. The main results provided by the model are heat losses in the receiver, HTF mass flow rate, receiver thermal efficiency, and pressure drops in the receiver. The selection of the optimal receiver tube dimension parameter is the result of an optimization procedure accounting for power losses due to the pumping of the HTF and thermal power losses. The selection of the number of axial and circumferential control volume significantly affects results and time expense of the receiver model. A discretization analysis is conducted to allow to select the correct discretization for each considered receiver size.

2.3. Piping

The mass flow rate and the pressure drop provided by the receiver model are used for the piping system design and off design evaluation. The piping model is developed in Matlab® as part of this thesis work. The model is able to design the whole piping system, to evaluate thermal and pressure losses and to estimate the costs. The model can be used for systems with any number of modules, any module size and layout, and with solar salts or liquid sodium as

heat transfer fluid. All the modules are assumed to have the same geometric and thermal characteristics. It is assumed that all the modules always operate in the same conditions and with the same mass flow rate. The design of the piping system significantly depends on the chosen value of HTF velocity. For this reason, the selection of this parameter is always the result of an optimization procedure accounting for pump electric power consumption and thermal power losses.

2.4. TES and power block

The thermal power data provided by the piping model are used in the thermal energy storage (TES) and power block models. The considered TES model uses solar salts as storage medium. A simple control strategy is applied: the system stores thermal power when it is provided in excess from the solar fields and provides thermal power to the power block when the power collected by the solar fields is insufficient. The storage system is considered as an ideal system with no thermal losses. The power block is based on a supercritical CO_2 Brayton cycle and operates with constant efficiency as long as the ambient temperature remains below the threshold of 30 °C. The modelling of these two subsystems is implemented in Matlab®.

2.5. Annual simulation

When the whole plant has been defined in all its subsystems (solar field, receiver, piping, TES, power block) the off-design behaviour of each of these subsystems must be assessed to estimate the annual energy production of the plant. The hourly energy production is estimated from the DNI data for each hour i of the year. The solar field optical efficiency is evaluated with a parametric analysis in SolarPILOT for different sun positions. The results are interpolated for the required values of

elevation and azimuth to evaluate optical efficiency for any sun position.

$$Q_{in,rec,i} = DNI_i \cdot A_{SF} \cdot \eta_{opt,i}$$

(1)

$$\eta_{opt,year} = \frac{\sum_{i=1}^{8760} Q_{in,rec,i}}{\sum_{i=1}^{8760} DNI_i \cdot A_{SF}} = \frac{Q_{in,rec,year}}{Q_{sun,year}}$$

(2)

The receiver off-design thermal efficiency is evaluated by simply scaling the values of the design heat flux map obtained from SolarPILOT from 20% to 120%. This approximation is possible because it has been proven in previous works [10] that the thermal efficiency of the receiver is only weakly influenced by the heat flux distribution. The main dependency is only on the overall receiver thermal input. The obtained thermal efficiencies and pressure drops are then interpolated for any needed receiver thermal input.

$$Q_{HTF,i} = Q_{in,rec,i} \cdot \eta_{th,i} \cdot N_{mod}$$

(3)

$$\eta_{th,year} = \frac{\sum_{i=1}^{8760} Q_{HTF,i}}{\sum_{i=1}^{8760} Q_{in,rec,i}} = \frac{Q_{HTF,year}}{Q_{in,rec,year}}$$

(4)

The piping off-design thermal efficiency and pump electric consumption are evaluated from the off-design values of mass flow rate provided by the receiver model. The model evaluates the piping system behaviour keeping the geometry defined in the design phase and computing the HTF speed for each piping subsection. The results obtained are then interpolated to obtain the piping thermal efficiency and the HTF pump electric power consumption for any needed value of thermal power input in the receiver.

$$Q_{HTF,net,i} = Q_{HTF,i} \cdot \eta_{pip,i}$$

(5)

$$\eta_{pip,year} = \frac{\sum_{i=1}^{8760} Q_{HTF,net,i}}{\sum_{i=1}^{8760} Q_{HTF,i}} = \frac{Q_{HTF,net,year}}{Q_{HTF,year}}$$

(6)

The net thermal power provided by the piping system enters the storage system and is used to operate the power block. The excess is stored and used when the power provided by the solar field is insufficient to operate the power block at rated capacity. The electric power production for each hour of the year and the annual energy production are evaluated.

$$P_{el,i} = Q_{in,PB,i} \cdot \eta_{PB,i}$$

(7)

$$P_{el,net,i} = P_{el,i} - W_{pump,i}$$

(8)

$$AEP = \sum_{i=1}^{8760} P_{el,net,i}$$

(9)

For the techno-economic optimization of the different configurations analysed in this work the levelized cost of heat (LCOH) and the levelized cost of electricity (LCOE) are evaluated.

$$LCOH = CRF \cdot \frac{Cost_{SF} + Cost_{tow} + Cost_{rec}}{Q_{HTF,year}}$$

(10)

$$LCOE = \frac{CRF \cdot CAPEX_{tot} + O\&M_f}{AEP} + O\&M_v$$

(11)

For the main components of the plant different. costs and cost correlations are found and the ones considered most suitable are used.

3   Case study

The case study of this thesis work focuses on a 5 MW_{el} plant where the solar field layout and the receiver geometry are initially developed starting from Vast Solar 1.2 MW_{th} modules. The plant is based on a recompressed sCO_2 power block. The closed loop sCO_2 cycle offers the potential of higher cycle efficiency versus superheated or supercritical steam cycles at temperatures relevant for CSP

applications. Liquid sodium is employed as heat transfer fluid. This allows to significantly increase the operating temperature of CSP systems to more than 700 °C and replace the steam Rankine cycle with the high efficiency supercritical CO_2 Brayton cycle [11]. An indirect storage system using molten salts as storage media is preferred to a direct liquid sodium storage system due to the safety risks associated to liquid sodium tanks and the high related cost [12]. Advanced molten based on NaCl (48% mol) and $MgCl_2$ (52% mol) are selected as storage media. Two systems with different operating temperature ranges are initially investigated: one with a turbine inlet temperature (TIT) of 550 °C and a design cycle efficiency of 37.5%, and one with a TIT of 700 °C and design cycle efficiency of 44%. The main cost assumptions are reported in Table 3.

3.1.　Part I – Cornfield module

The first part of the analysis investigates the optical performances of a cornfield module similar to the one used by Vast Solar and investigates some variations in the heliostat disposition. Modular and single field plants with optimized solar multiple (SM) and TES size evaluated with two different operating temperatures and compared. The configurations operating at higher temperatures are selected for the rest of the analysis due to better performances. In the next step the receiver size and tower height are changed with respect to the ones used at Jemalong pilot plant, and they are optimized as function of LCOH. Then SM and TES size are optimized as function of LCOE (Figure 2).
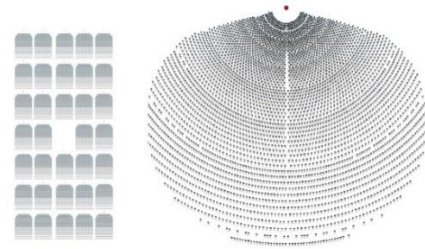

Figure 2 Best modular configuration (34 modules) and best single field configuration

3.2.　Part II – Module optimization

In the second part, to furtherly increase the modular plant performances, module configurations different from the one used by Vast Solar are investigated: a rectangular shape polar module with radial layout of the heliostats, and a polar solar field with no shape limitations. From the obtained results it is decided to discard the cornfield module. A surrounded module layout is instead added for the next analysis (Figure 3). To furtherly improve the modular plant performances the size of the modules is investigated. For each one of the three layouts the power delivered to the receiver is varied from 1 MW_{th} to 10 MW_{th} with a step increase of 1 MW_{th}. For each layout and rated power, the tower height and the receiver size are optimized computing the LCOH. When the best solar module geometry is identified for each combination of layout and size the solar multiple and the TES size are optimized computing the LCOE. This procedure provides for each combination the best modular plant. These modular plants are compared with two single field plants.
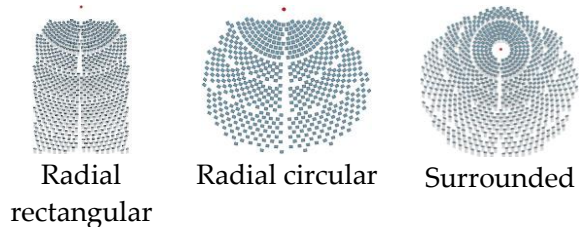

Radial rectangular　Radial circular　Surrounded

Figure 3 Layout configurations considered for the modular plant after the cornfield layout is discarded

4   Results

4.1.   Part I – Cornfield module

Using the cornfield module layout two different temperature ranges are investigated. The solar multiple is optimized by changing the number of modules, in the modular configurations, and by changing the field size in the case of the single field configurations (Table 1).

	Modular 430-580°C	Single field 430-580°C	Modular 550-730°C	Single field 550-730°C
Solar multiple (optimized)	3.4	2.75	3.5	2.85
TES size [h] (optimized)	14	12	14	13
LCOE [$/MWh]	176	180	164	167

Table 1 Main parameters and performance indicators of the four optimal configurations

The systems operating in the temperature range 550-730°C provide better performances at lower cost reaching ~7% lower LCOE with respect to the systems operating at lower temperatures, thanks to the higher power block efficiency. For this reason, only the 550-730°C case is considered for the next analysis. To improve the performances of the modular system the tower height and receiver size are optimized as function of LCOH (Figure 4). The same is done for the single field configuration. Higher tower heights provide better optical efficiency but higher costs. Bigger receiver sizes increase the optical efficiency and the costs and reduce the thermal efficiency.
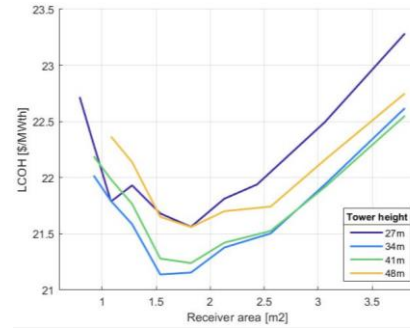

Figure 4 LCOH as function of receiver size and tower height for the modular layout

The modular configuration provides a slightly higher annual energy production with respect to the single field configuration, thanks to the higher optical efficiency Nevertheless, the higher investment cost of the modular systems provides a final LCOE which is very close to the LCOE of the single field system (Table 2).
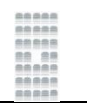
Number of modules	34	-
Tower height (Optimized)	34 m	100 m
Receiver size (Optimized)	1.25 x 1.25 m	5 x 5 m
Solar multiple (Optimized)	3.7	3.0
TES size (Optimized)	15 h	13 h
LCOE [$/MWh]	153	152

Table 2 Main parameters and performance indicators of the two optimal configurations

The modular configuration shows higher total investment costs with respect to their single field counterparts, mainly because of the cost of the receivers and of the piping system To furtherly investigate the possible advantages of the modularity of CSP plants heliostat dispositions alternative to the cornfield one and different module sizes are investigated.

4.2.   Part II – Module optimization

A radial rectangular, a radial circular, and a surrounded layout (Figure 3) are used to investigate the effect on performances and costs of different module sizes. For each power and each layout different tower heights and receiver sizes are evaluated.

The annual optical efficiency improves significantly increasing receiver area and tower height. At the same time the annual optical efficiency decreases considerably with the size of the module, as heliostats are placed at more distance from the tower (Figure 5).
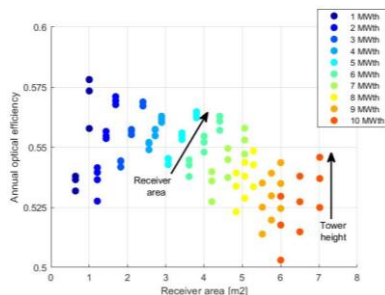

Figure 5 Annual optical efficiency as function of receiver area for the radial rectangular layout

The surrounded modules present higher optical efficiency with respect to the polar layouts, as heliostats have better positioning (Figure 6). For the same reason the radial circular layout presents slightly better optical performances with respect to the radial rectangular layout.
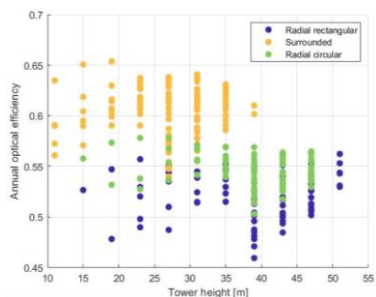

Figure 6 Annual optical efficiencies of the three layouts

Thermal efficiency generally reduces by increasing the receiver area. Increasing the tower height has a very limited negative effect on the receiver thermal efficiency The cylindrical receiver model used in the surrounded configuration leads to lower thermal efficiencies with respect to the billboard receiver model used in the polar configurations (Figure 7). This is due to the limit on the maximum allowed flux on the receiver surface: as the flux is less evenly distributed bigger receivers are necessary to remain below the flux limit, thus increasing the receiver area and reducing the average flux and the thermal efficiency.
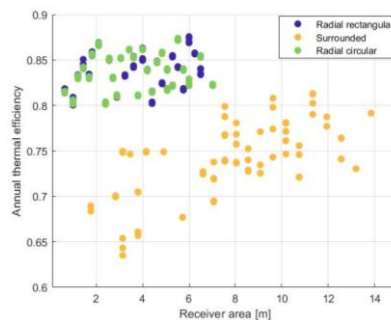

Figure 7 Annual thermal efficiencies of the three layouts

From the obtained results, for each one of the investigated configurations, the optical efficiency and the thermal efficiency can be estimated for any value of tower height, receiver area, and module power around the computed points.

The LCOH for the different investigated modular configurations is then evaluated. For the polar configurations very small modules, around 1-2 MW_{th}, and very large modules, around 9-10 MW_{th}, present higher LCOH values with respect to modules in the mid-size range, as a consequence of the lower optical-thermal efficiency. In the case of the surrounded layout increasing the module size reduces the LCOH, as thermal efficiency improves significantly. The LCOH obtained for the three modular layouts are compared with the LCOH obtained for two single field plants (Figure 8).
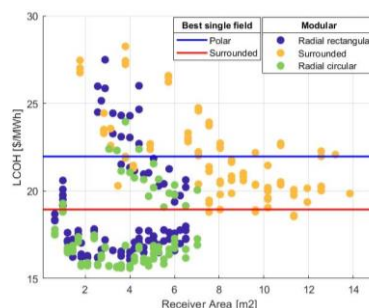

Figure 8 LCOH values of the three modular layouts and the two optimal single field configurations

For each module layout and each module size the optimal values of tower height and

receiver size that minimize the LCOH are identified (Figure 9). Also, the values that minimize the optical-thermal efficiency are reported. In the case of the radial rectangular and the radial circular layouts the values of receiver area and tower height that optimize the LCOH, and the values that optimize the optical-thermal efficiency are very close. In the case of the surrounded layout the values of receiver area and tower height that optimized the LCOH are significantly lower than the values that optimize the optical-thermal efficiency. In the surrounded layout the improvement of optical-thermal performances is not enough to compensate the cost increase associated with higher towers and bigger receivers.
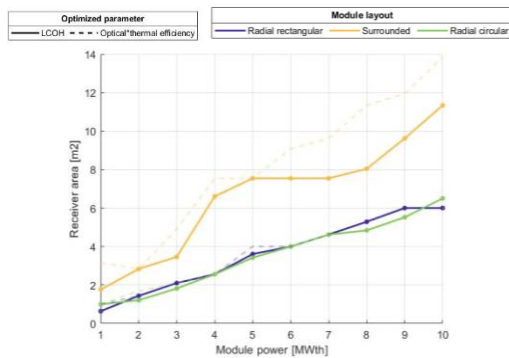

Figure 9 Receiver area that minimizes the LCOH for each module layout

For each one of the 30 selected optimal geometries (10 for each module layout, 1 for each module size) the solar multiple is changed adjusting the number of modules, and the corresponding piping thermal efficiency and solar to electric efficiency (STE) are evaluated. The piping efficiency mainly depends on the number of modules: a higher number of modules implies a more extended piping network and increased thermal losses. This effect is particularly relevant for a small number of modules (1-6). Increasing the number of modules, the piping efficiency becomes more sensitive to the size of the modules (Figure 10). The same trends are shown for the solar to electric efficiency.
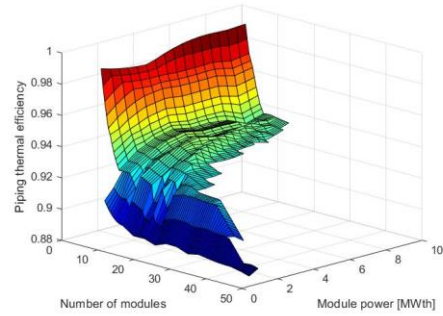

Figure 10 Piping annual thermal efficiency as function of number of modules and power of the module for the radial circular layout

For each module layout, each module size, and each solar multiple the TES size is varied and the LCOE is computed to identify the optimal configuration. The optimal TES size mainly depends on the SM, which determines the amount of excess heat available for the storage. Module size has a limited effect, as the effect SM prevails on the effect of the extension of the piping system (Figure 11).
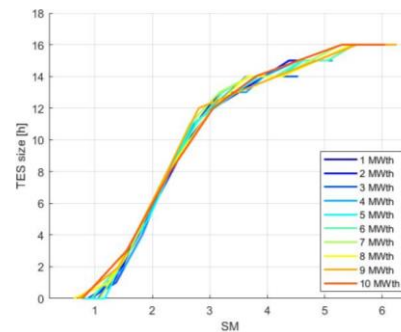

Figure 11 optimal TES size as function of SM and module power for the radial circular layout

With the optimized TES size for each module power the optimal solar multiple is identified (Figure 12). For any module layout and module size the optimal solar multiple is in the range 3-4. The lower optimal solar multiple for very small and very big module sizes reflects the piping efficiency trends discussed before: higher solar multiple would significantly affect the piping efficiency and therefore lower optimal SM values are obtained.
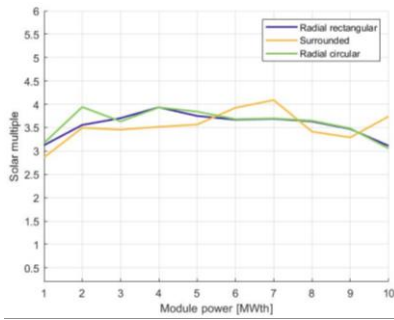
Figure 12 Optimal solar multiple for each considered layout

The surrounded module reaches LCOE values higher than the one obtained with a corresponding single field plant (Figure 13), mainly because of the higher costs associated to the receiver and to the piping system. In the case of the polar layouts the modular configuration allows to reach noticeably lower LCOE values with respect to the single field counterparts, thanks to the higher solar to electric efficiency. In the case of the radial rectangular and the radial circular layouts the optimization of TES size and solar multiple leads to very similar LCOE values, almost independently from the module size.
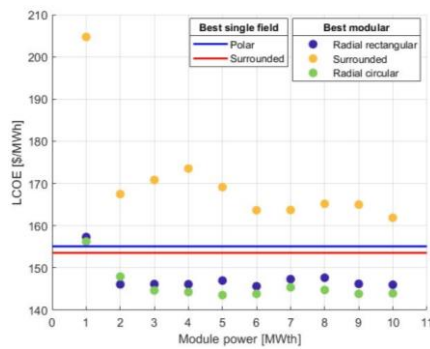

Figure 13 LCOE values of the optimal modular and single field configurations

The best radial rectangular configuration, with 8 modules of 6 MW$_{th}$ of power, and optimal solar multiple equal to 3.7, reaches a LCOE of 143.6 $/MWh. The best radial circular configuration, with 10 modules of 5 MW$_{th}$ of power, and optimal solar multiple equal to 3.8, reaches a LCOE of 145.6 $/MWh. The best surrounded configuration, with 5 modules of 10 MW$_{th}$

of power, and solar multiple equal to 3.7, reaches a LCOE of 161.8 $/MWh.

5   Conclusion

This thesis work investigated from a techno-economic perspective different possible modular configuration for a CSP tower plant. A radial circular modular configuration, formed by 10 modules of 5 MW$_{th}$ of power, proved to be the best candidate with a LCOE of 143.6 $/MWh, a value 6.5 % lower than the LCOE obtained with a single field configuration. Also, the obtained results provide possible selection criteria for the optimal number of modules, the optimal TES size, and the optimal module size for a modular CSP plant. It is important to note that the modelling of solar field, receiver, and piping system was implemented to have a high degree of accuracy, while the TES and the power block system were treated with a much simpler approach, neglecting heat exchangers and thermal losses in the storage tanks. This approach was intended to focus the analysis on the subsystems that are different between the modular and the single field configurations. It is important to underline that the obtained values of LCOH and LCOE strongly depend on the assumed costs for the different system components. Due to the high uncertainty associated to cost correlations and to the difficulty to retrieve accurate and reliable cost data the economic parameters are subjected to significant variability. It is also important to stress that possible cost reductions due to the modularization of system components were not considered and could play a relevant role in making modular configurations more convenient. Future works should investigate the effect of heliostat size on system costs and performances. Also, the receiver aspect ratio should be varied to evaluate possible advantages in terms of optical-thermal

efficiency and costs, especially for the surrounded layouts. Plants with power blocks of increased size, e.g., 25-50 MWel, should be investigated, as the constant optical efficiency obtained with the modular approach could provide a more significant advantage with respect to the single field configurations, where solar fields of increasing size are required.

References

[1] J. H. Lim, B. B. Dally, A. Chinnici e G. J. Nathan, «Techno-economic evaluation of modular hybrid concentrating solar power systems,» *Energy,* vol. 129, pp. 158-170, 2017.

[2] L. Crespo e F. Ramos, «Making central receiver plants modular, more efficient and scalable,» *AIP Conference Proceedings,* vol. 2303, 2020.

[3] C. Tyner e D. Wasyluk, «eSolar's Modular, Scalable Molten Salt Power Tower Reference Plant Design,» *Energy Procedia,* pp. 1563-1572, 01 January 2014.

[4] L. Crespo, A. Ramos, F. Ramos e D. Crespo, «Revisiting field layout designs for large STE tower plants,» *AIP Conference Proceedings,* vol. 2033, 2018.

[5] M. Puppe, S. Giuliano, C. Frantz, R. Uhlig, R. Flesch, R. Schumacher, W. Ibraheem, S. Schmalz, B. Waldmann, C. Guder, D. Peter, C. Schwager, C. T. Boura, S. Alexopoulos e M. Spiegel, «Techno-economic optimization of molten salt solar tower plants,» *AIP Conference Proceedings,* vol. 2033, 2018.

[6] Lloyd Energy Systems Pty Ltd, «Lake Cargelligo Solar Thermal Project Final Pubñic Report,» 2011.

[7] C. W. Wood e K. Drewes, «Vast Solar: improving performance and reducing cost and risk using high temperature modular arrays and sodium heat transfer fluid,» in *SolarPACES Conference*, 2019.

[8] M. J. Wagner e T. Wendelin, «SolarPILOT: A power tower solar field layout and characterization tool,» *Solar Energy,* vol. 171, pp. 185-196, 2018.

[9] E. Morosini, G. Gentile, M. Binotti e G. Manzolini, «Techno-economic assessment of small-scale solar tower plants with modular billboard receivers and innovative power cycles,» in *ATI Annual Congress*, Bari, 2022.

[10] G. Gentile, G. Picotti, M. Binotti, M. E. Cholette e G. Manzolini, «Dynamic thermal analysis and creep-fatigue lifetime assessment of solar tower external receivers,» *Solar Energy,* 2022.

[11] U.S. Department of Energy, «Quadrennial Technology Review 2015 - Supercritical Carbon Dioxide Brayton Cycle,» 2016.

[12] R. Jacob, M. Belusko, A. Inés Fernández, L. F. Cabeza, W. Saman e F. Bruno, «Embodied energy and cost of high temperature thermal energy storage systems for use with concentrated solar power plants,»

Applied Energy, vol. 180, pp. 586-597, 2016.

Appendix

Cost item	Value
Tower (steel lattice) H < 45 m	$\frac{H[m]}{1000}$ M$
Tower (steel monopole) H > 45 m	$1.50227 - 0.00879597 \cdot H[m] + 0.000189709 \cdot H^2$ M$
Receiver (1)	135 $/kW$_{th}$
Receiver (2)	$52.0685 \cdot \frac{A_{rec}\,[m^2]}{560.77}$
Piping	See Section 2.7, Table 12
TES (430-580 °C)	$(10.74 + 10.74 + 9.75) \cdot \left(\frac{V[m^3]}{15650}\right)^{0.8}$ M$
TES (550-730 °C)	$(10.74 + 19.34 + 9.75) \cdot \left(\frac{V[m^3]}{15650}\right)^{0.8}$ M$
Power block (TIT 550 °C)	2493 $/kW$_{el}$
Power block (TIT 700 °C)	2543 $/kW$_{el}$
O&M fixed	65 $/kW$_{el}$/y
O&M variable	3.5 $/MWh$_{el}$
Indirect costs	20% of CAPEX
Plant lifetime	30 y
Discount rate	8%

Table 3 Cost assumptions for the comparison of the plants